AD-A178 492 NUMERICAL SIMULATION OF SUPERSONIC FLOW OVER A ROTATING BAND USING FLOWFIELD BLANKING(U) ARMY BALLISTIC RESEARCH LAB ABERDEEN PROVING GROUND MD J SAHU DEC 86 1/1

UNCLASSIFIED BRL-MR-3561 F/G 20/4 NL

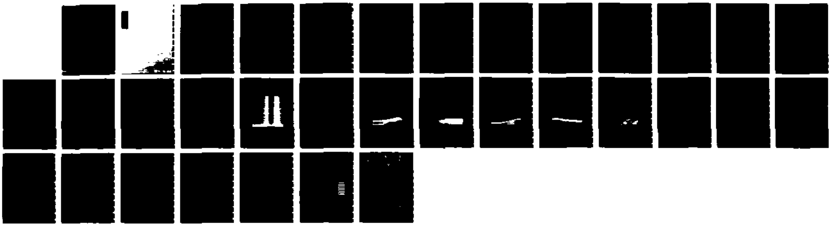

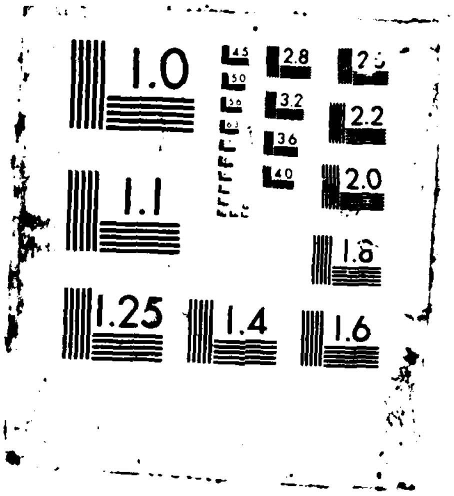
1.0
2.8
3.2
2.2
3.6
4.0
2.0
1.1
1.8
1.25
1.4
1.6

UNCLASSIFIED
SECURITY CLASSIFICATION OF THIS PAGE

REPORT DOCUMENTATION PAGE

Form Approved
OMB No 0704-0188
Exp Date Jun 30, 1986

1a REPORT SECURITY CLASSIFICATION UNCLASSIFIED	1b RESTRICTIVE MARKINGS AD-A178 492
2a SECURITY CLASSIFICATION AUTHORITY	3 DISTRIBUTION/AVAILABILITY OF REPORT Approved for public release, distribution unlimited.
2b DECLASSIFICATION/DOWNGRADING SCHEDULE	
4 PERFORMING ORGANIZATION REPORT NUMBER(S) BRL-MR-3561	5. MONITORING ORGANIZATION REPORT NUMBER(S)
6a. NAME OF PERFORMING ORGANIZATION US Army Ballistic Research Laboratory 6b. OFFICE SYMBOL (If applicable) SLCBR-LF	7a. NAME OF MONITORING ORGANIZATION
6c. ADDRESS (City, State, and ZIP Code) Aberdeen Proving Ground, Maryland 21005-5066	7b. ADDRESS (City, State, and ZIP Code)
8a. NAME OF FUNDING/SPONSORING ORGANIZATION 8b. OFFICE SYMBOL (If applicable)	9 PROCUREMENT INSTRUMENT IDENTIFICATION NUMBER
8c. ADDRESS (City, State, and ZIP Code)	10. SOURCE OF FUNDING NUMBERS

PROGRAM ELEMENT NO.	PROJECT NO	TASK NO	WORK UNIT ACCESSION NO
62618A	1L162618AH80	00	AJ

11. TITLE (Include Security Classification)

NUMERICAL SIMULATION OF SUPERSONIC FLOW OVER A ROTATING BAND USING FLOWFIELD BLANKING

12. PERSONAL AUTHOR(S)
JUBARAJ SAHU

13a. TYPE OF REPORT	13b. TIME COVERED	14 DATE OF REPORT (Year, Month, Day)	15. PAGE COUNT
Memorandum Report	FROM ______ TO ______		

16. SUPPLEMENTARY NOTATION

17. COSATI CODES

FIELD	GROUP	SUB-GROUP
01	01	
19	04	

18. SUBJECT TERMS (Continue on reverse if necessary and identify by block number)
Supersonic Flow, Navier-Stokes, Sharp Corners, Flowfield Blanking, Rotating Band.

19 ABSTRACT (Continue on reverse if necessary and identify by block number)

Implicit, approximately factored, finite difference codes have been developed for solving the Navier-Stokes equations in general body-fitted coordinates. For a protuberance such as the rotating band on artillery shell, sharp geometric variations exist which make it extremely difficult to generate body-conforming grids while preserving the sharp corners. Using wrap-around grids for such cases introduces geometric errors and may lead to degradation of computational efficiency and accuracy. This report describes the development and application of a computational procedure using flowfield blanking to compute the flow over a rotating band at supersonic speed with no geometric error.

20 DISTRIBUTION/AVAILABILITY OF ABSTRACT [X] UNCLASSIFIED/UNLIMITED [ ] SAME AS RPT [ ] DTIC USERS	21 ABSTRACT SECURITY CLASSIFICATION UNCLASSIFIED
22a NAME OF RESPONSIBLE INDIVIDUAL JUBARAJ SAHU	22b TELEPHONE (Include Area Code) SLCBR-LF-R 22c OFFICE SYMBOL 301-278-3707

DD FORM 1473, 84 MAR — 83 APR edition may be used until exhausted. All other editions are obsolete

UNCLASSIFIED
SECURITY CLASSIFICATION OF THIS PAGE

TABLE OF CONTENTS

LIST OF FIGURES

I. INTRODUCTION

In recent years, a considerable research effort has been focused on the development of modern predictive capabilities for determining the aerodynamics of projectiles. The time-dependent Navier-Stokes computational technique has been used[1-2] to compute the flow over projectiles at transonic speeds. For supersonic flows, space-marching parabolized[3] Navier-Stokes computational technique can be effectively used. However, this technique fails for flows containing longitudinal flow separation. In such cases, which are frequently encountered in projectile aerodynamic simulations, the time-dependent Navier-Stokes technique needs to be used.[4-5]

The time-dependent Navier-Stokes equations can be solved in a generalized body-fitted coordinate system. Many actual projectile configurations contain sharp corners and steps. These sharp geometric variations make it extremely difficult to generate body-conforming grids while preserving the sharp corners. The grid lines are wrapped around the corners and, in many cases, such wrap around grids are skewed near these corners and steps. Using such grids introduces geometric errors and sometimes leads to loss in both the computational efficiency and accuracy. In this report we develop and apply a flowfield blanking procedure which allows computation of practical flows of interest with no geometric error since it models the corners and steps exactly.

To avoid geometric errors one can blank out the flowfield in specific regions in the computational domain. Examples where such blanking can be useful are shown in Figure 1. Continuous straight line grids can be used for these cases and the hatched regions are the ones where the flowfield is to be blanked out. This procedure, thus, preserves the sharp corners and steps. In addition to zeroing out the flowfield inside the hatched regions, additional changes must be made in the boundary conditions and the computational algorithm near these surfaces. These changes are described in a later section. This technique can be tested with the simple problem of flow over a rotating band. The rotating-band, which is a protuberance on the artillery shell, imparts spin to a shell during launch. However, it does contribute a small unwanted drag in free flight. A schematic of the rotating-band flowfield is shown in Figure 2. It shows the expected recirculation regions in front of and behind the band and the associated compressions and expansion waves. A numerical solution is obtained for this problem at $M_\infty = 3.0$ and $\alpha = 0$.

II. COMPUTATIONAL TECHNIQUE

1. GOVERNING EQUATIONS

The complete set of time-dependent generalized axisymmetric thin-layer Navier-Stokes equations is solved numerically to obtain a solution to this problem. The numerical technique used is an implicit finite-difference scheme. Although time-dependent calculations are made, the transient flow is not of primary interest at the present time. The steady flow is the desired result which is obtained in a time asymptotic fashion.

The azimuthal-invariant (or generalized axisymmetric) thin-layer Navier-Stokes equations for curvilinear coordinates ξ, η and ζ can be written as:[1]

$$\frac{\partial \hat{q}}{\partial \tau} + \frac{\partial \hat{E}}{\partial \xi} + \frac{\partial \hat{G}}{\partial \zeta} + \hat{H} = Re^{-1}\,\frac{\partial \hat{S}}{\partial \zeta} \tag{1}$$

where

$\xi = \xi(x,y,z,t)$ is the longitudinal coordinate

$\eta = \eta(y,z,t)$ is the circumferential coordinate

$\zeta = \zeta(x,y,z,t)$ is the near normal coordinate

$\tau = t$ is the time

and

$$\hat{q} = J^{-1}\begin{bmatrix} \rho \\ \rho u \\ \rho v \\ \rho w \\ e \end{bmatrix}, \quad \hat{E} = J^{-1}\begin{bmatrix} \rho U \\ \rho u U + \xi_x p \\ \rho v U + \xi_y p \\ \rho w U + \xi_z p \\ (e+p)U - \xi_t p \end{bmatrix}, \quad \hat{G} = J^{-1}\begin{bmatrix} \rho W \\ \rho u W + \zeta_x p \\ \rho v W + \zeta_y p \\ \rho w W + \zeta_z p \\ (e+p)W - \zeta_t p \end{bmatrix},$$

$$\hat{H} = J^{-1}\begin{bmatrix} 0 \\ 0 \\ \rho v[R_\xi(U-\xi_t) + R_\zeta(W-\zeta_t)] \\ -\rho v R\phi_\eta(V-\eta_t) - p/(R\phi_\eta) \\ 0 \end{bmatrix}$$

$$\hat{S} = \begin{bmatrix} 0 \\ \mu(\zeta_x{}^2 + \zeta_y{}^2 + \zeta_z{}^2)u_\zeta + (\mu/3)(\zeta_x u_\zeta + \zeta_y v_\zeta + \zeta_z w_\zeta)\zeta_x \\ \mu(\zeta_x{}^2 + \zeta_y{}^2 + \zeta_x{}^2)v_\zeta + (\mu/3)(\zeta_x u_\zeta + \zeta_y v_\zeta + \zeta_z w_\zeta)\zeta_y \\ \mu(\zeta_x{}^2 + \zeta_y{}^2 + \zeta_z{}^2)w_\zeta + (\mu/3)(\zeta_x u_\zeta + \zeta_y v_\zeta + \zeta_z w_\zeta)\zeta_z \\ \{(\zeta_x{}^2 + \zeta_y{}^2 + \zeta_y{}^2)[(\mu/2)(u^2 + v^2 + w^2)_\zeta + \kappa Pr^{-1}\,(\gamma-1)^{-1}(a^2)_\zeta] \\ + (\mu/3)(\zeta_x u + \zeta_y v + \zeta_z w)(\zeta_x u_\zeta + \zeta_y v_\zeta + \zeta_z w_\zeta)\} \end{bmatrix}$$

The velocities

$$U = \xi_t + \xi_x u + \xi_y v + \xi_z w$$

$$V = \eta_t + \eta_x u + \eta_y v + \eta_z w \qquad (2)$$

$$W = \zeta_t + \zeta_x u + \zeta_y v + \zeta_z w$$

represent the contravariant velocity components.

The Cartesian velocity components (u, v, w) are nondimensionalized with respect to a_∞ (free stream speed of sound). The density (ρ) is referenced to ρ_∞ and total energy (e) to $\rho_\infty a_\infty^2$. The local pressure is determined using the equation of state,

$$p = (\gamma - 1)[e - 0.5\rho(u^2 + v^2 + w^2)] \qquad (3)$$

where γ is the ratio of specific heats.

While Equation (1) contains only two spatial derivatives, it retains all three momentum equations, thus allowing a degree of generality over the standard axisymmetric equations. In particular, the circumferential velocity is not assumed to be zero, thus allowing computations for spinning projectiles or swirl flow to be accomplished.

2. COMPUTATIONAL ALGORITHM

The azimuthal-invariant, thin-layer Navier-Stokes equations are solved using an implicit approximate factorization finite difference scheme in delta form.[6] An implicit method was chosen because, for viscous flow problems, it permits a time step much greater than that allowed by explicit schemes. The Beam-Warming implicit algorithm has been used in various applications[1-9] for the equations in general curvilinear coordinates. The algorithm is first-order accurate in time and second- or fourth-order accurate in space. The equations are factored (spatially split), which reduces the solution process to one-dimensional problems at a given time level. Central difference operators are employed and the algorithm produces block tridiagonal systems for each space coordinate. The main computational work is contained in the solution of these block tridiagonal systems of equations. For the computation of turbulent flows, the two-layer algebraic Baldwin-Lomax turbulence model[10] is used.

3. FINITE-DIFFERENCE EQUATIONS

The implicit, approximately factored algorithm developed by Beam-Warming[6] has the form:

$$[I + h\delta_\xi \hat{A}^n + D_\xi^{(2)}][I + h\delta_\zeta \hat{C}^n - hRe^{-1}\ \delta_\zeta J^{-1}\ \hat{M}^n J + D_\zeta^{(2)}]\Delta \hat{q}^n$$

$$= -h[\delta_\xi \hat{E}^n + \delta_\zeta \hat{G}^n - Re^{-1}\ \delta_\zeta \hat{S}^n + \hat{H}^n + D^{(4)}] \tag{4}$$

where the explicit fourth-order dissipation is:

$$D^{(4)} = -\varepsilon_e \Delta t J^{-1}[(\nabla_\xi \Delta_\xi)^2 + (\nabla_\zeta \Delta_\zeta)^2] J\ \hat{q}^n$$

and the implicit second-order dissipation terms are:

$$D_\xi^{(2)} = -\ \varepsilon_i \Delta t J^{-1}(\nabla_\xi \Delta_\xi) J$$

$$D_\zeta^{(2)} = -\ \varepsilon_i \Delta t J^{-1}(\nabla_\zeta \Delta_\zeta) J\ .$$

The fourth-order explicit dissipation is used to control non-linear instabilities whereas the implicit dissipation is included to stabilize the explicitly treated fourth-difference terms. The parameter ε_e is 0(1) and the parameter ε_i is two to three times ε_e. The Jacobian matrices $\hat{A} = \frac{\partial \hat{E}}{\partial \hat{q}}$, $\hat{C} = \frac{\partial \hat{G}}{\partial \hat{q}}$ along with coefficient matrix $\hat{M}$ obtained from linearization of $\hat{S}$ are described in detail in Reference 8.

To suppress high frequency components that appear in regions containing severe pressure gradients, e.g., shocks or stagnation points, a switching dissipation model is used. This switching model is similiar to the model used by Pulliam[9] and uses a fourth-order dissipation in smooth regions and switches to a second-order dissipation in regions containing high pressure or density gradients. The dissipation term $D^{(4)}$ on the right hand side of Equation (4) can be written in this model as:

$$\frac{\Delta t}{J}\ ||A_\infty||\ [\delta\ \varepsilon_d\ |\frac{\Delta\nabla\rho}{\langle\rho\rangle}|\ \delta\ J\ q - \delta\ \varepsilon_e\ \delta\Delta\nabla\ J\ q] \tag{5}$$

where the first term is the second-order dissipation and the second term contains the fourth-order dissipation. The coefficients ε_d and ε_e are the associated coefficients for the second-order and fourth-order dissipation, respectively. The coefficient ε_d is fifty to hundred times ε_e and Δ and ∇ are the one-sided forward and backward finite-difference operators. Note that the fourth-order dissipation is non-linear in that the coefficient is not a constant and is scaled by spectral radius $||A_\infty||$. The two terms in Equation (5) are of the form $\delta\alpha\delta\beta$ where:

$$(\delta\ \alpha\ \delta\ \beta)_j = \left(\frac{\alpha_{j+1} + \alpha_j}{2}\right)(\beta_{j+1} - \beta_j) + \left(\frac{\alpha_j + \alpha_{j-1}}{2}\right)(\beta_j - \beta_{j-1})$$

Fourth-order dissipation is used if $\varepsilon_e > \varepsilon_d \left|\frac{\nabla\Delta\rho}{\langle\rho\rangle}\right|$ and the dissipation is switched to second-order if $\varepsilon_e < \varepsilon_d \left|\frac{\nabla\Delta\rho}{\langle\rho\rangle}\right|$. The pressure gradient is used in the normal direction in this switching control whereas density, as shown in Equation (5), is used in the longitudinal direction. In addition, a space varying[9] Δt procedure is used where the time step used is given as:

$$\Delta t = \frac{(\Delta t)_{ref}}{1 + \sqrt{J}} \tag{6}$$

where J is the Jacobian of the transformation and $(\Delta t)_{ref}$ is a reference time step.

4. FLOWFIELD BLANKING

The idea is to avoid geometric errors that may arise from wrap around grids. Instead, we use straight line grids as shown schematically in Figure 3. For the rotating band problem, the zone ABCD is part of the body and the flowfield in this zone must be blanked out in the computational domain. As shown in Figure 3, the sharp corners and steps ahead of and behind the band are preserved and no approximation is made. It is also necessary to apply boundary conditions on the zonal surfaces AB, BC and CD. The no-slip boundary conditions are used at these boundaries along with zero gradients for pressure and density. In addition, at neighboring points to these boundaries, we use second-order spatial difference and smoothing. The block tridiagonal matrix structure has been modified for continuous integration sweeps through such zones. For example, the block tridiagonal matrix in the ξ direction takes the following form (after setting $\varepsilon_i = 0$ to simplify the illustration)

$$\begin{array}{cccccc}
 & I & A_3 & & & \\
-A_2 & I & A_4 & & & \\
\ddots & \ddots & \ddots & & & \\
-A_{J1-2} & I & A_{J1} & & & \\
 & 0 & I & 0 & & \\
 & \ddots & \ddots & \ddots & & \\
 & & 0 & I & 0 & \\
 & & -A_{J2} & I & A_{J2+2} & \\
 & & \ddots & \ddots & \ddots & \\
 & & & -A_{JMAX-2} & I &
\end{array}
\begin{array}{c}
\Delta q_2 \\ \Delta q_3 \\ \vdots \\ \vdots \\ \Delta q_{J1} \\ \vdots \\ \Delta q_{J2} \\ \vdots \\ \vdots \\ \Delta q_{JMAX-1}
\end{array}
=
\begin{array}{c}
RHS_2 \\ RHS_3 \\ \vdots \\ \vdots \\ 0 \\ \vdots \\ \vdots \\ 0 \\ \vdots \\ RHS_{JMAX-1}
\end{array} \tag{7}$$

Here A's denote the quantity $\frac{\Delta t}{2\Delta\xi}\hat{A}$ and I is a 5 × 5 identity matrix. Note the appearance of the uncoupled block tridiagonals between J = J1 and J2 corresponding to lines AB and DC, respectively. The rows at J1 and J2 are particularly simple because boundary conditions are updated explicitly at the end of inversions. All the changes described in this section were easily implemented in a modular fashion into an existing code for projectile flow computations. One simply fills the block tridiagonal matrix ignoring the zone. Elements in the rows inside the zone are then overloaded as shown above. The flowfield blanking affects the block tridiagonal matrix in the ζ direction similarly. Although, we have only one zone for the rotating band case, changes have been made in the code to blank out multiple zones.

III. RESULTS

All the numerical computations were made at M_∞ = 3.0 and α = 0. The projectile configuration with the rotating band which was used in this study is shown in Figure 4. This model is a cone-cylinder configuration with a 13.1° cone angle. The band height is .04 D and the width is .505 D. The same model was used in the experiments[11] which were conducted in the US Army Chemical Research Development and Engineering Center's Supersonic Wind Tunnel. Surface pressure measurements have been made ahead of and behind the band which are used to compare with the numerical results.

Since the freestream flow is supersonic, the space marching Parabolized Navier-Stokes code[3] was used to compute the solution over the forebody of the projectile (See Figure 5). This generated a solution at a station 30 band heights ahead of the band which was then used as an upstream boundary condition for the computation of the flowfield containing the rotating band. For this part of the flowfield which includes the band, the unsteady or time-dependent Navier-Stokes computational technique described earlier was used. Such composite solution technique allowed a large number of grid points to be used in the vicinity of the band.

The computational grid used for the numerical calculations is shown in Figure 6. It consists of 130 points in the longitudinal direction and 60 points in the normal direction. The grid points are clustered near the surface of the cylindrical part with a minimum spacing of .00002 D. The resolution of grid points on the top of the band is not as fine. Grid points in the longitudinal direction are clustered near the upstream and downstream corners of the rotating band where appreciable changes in the flow variables are expected. In Figure 6, the grid lines inside the band are omitted to show the position of the band; however, in the actual grid used in the computations, there are continuous grid lines inside the band and those are the lines where the flowfield blanking procedure is used.

For comparison purposes, a numerical solution is first obtained for flow over the cylindrical part of the projectile without the rotating band at M_∞ = 3.0 and α = 0. The computed surface pressure coefficient is plotted in Figure 7 as a function of longitudinal position. The computed result is in very good agreement with experimental data.[11]

Numerical results obtained for the rotating band case are presented next. Figure 8a shows the velocity vector field in front of the band and as expected, it shows the recirculatory flow in that region. As shown in this figure, the flow seems to accelerate as the corner of the band is approached. Figure 8b shows the velocity vectors behind the band. The flow expands at the corner of the band. A recirculation region can be observed clearly. Figures 9a and 9b show the stream function contours ahead of and behind the band, respectively. The recirculatory flow regions can be clearly seen in these figures. The reverse flow region extends about four band heights ahead of the band and the reattachment point is less than a quarter of the height of the band from the corner. The size of the recirculation bubble behind the band is a little smaller than the one ahead of the band. The flow seems to separate slightly below the band corners and reattaches about 3.5 band heights downstream. Figure 10 shows the pressure contours for this case. One can also see a separation shock wave ahead of the band. The shock wave is located just ahead of the flow separation region. The strong flow expansions at both the band corners can be clearly seen. The expansions at the downstream corner is followed by a recompression shock. The surface pressure coefficient for the band case is shown in Figure 11 as a function of the axial position. The solid line is the computed result, the dashed line is the result obtained for the case without the band and the circles are the experimental data for the band. There is a considerable change in the pressure due to the presence of the band. The sharp rise in pressure ahead of the band is associated with the shock wave which actually precedes the separation point of the boundary layer flow. The flow then expands at the corner and pressure drops. No significant change in pressure occurs on the top of the band. At the backward step of the band, the flow expands again which results in the sharp decrease in the pressure. This is followed by a more gradual return to the ambient pressure downstream. The computed surface pressure is in good agreement with the experimental data measured ahead of and behind the band. The small discrepancy found in the comparison could be due to the turbulence model used.

IV. CONCLUDING REMARKS

The Navier-Stokes computational technique has been used in conjunction with a flowfield blanking procedure for numerical simulation where the sharp corners and steps exactly modeled, thereby, avoiding any possible source of geometric errors. This procedure has been applied to the flow over a rotating band at supersonic speed.

Computed results have been obtained for $M_\infty = 3.0$ and $\alpha = 0$ and compared with available experimental data. The results show the recirculation region both ahead of and behind the rotating-band as well as the associated compression and expansion waves. The computed surface pressures for both cases, with and without the band, are in fairly good agreement with experimental data. The present numerical procedure is simple to use and seems to predict the flowfield correctly. Further work is needed to extend this technique to predict three dimensional flow fields. In addition, a parametric study will be conducted in future to predict the effect of the rotating-band on the aerodynamic coefficients for artillery shell.

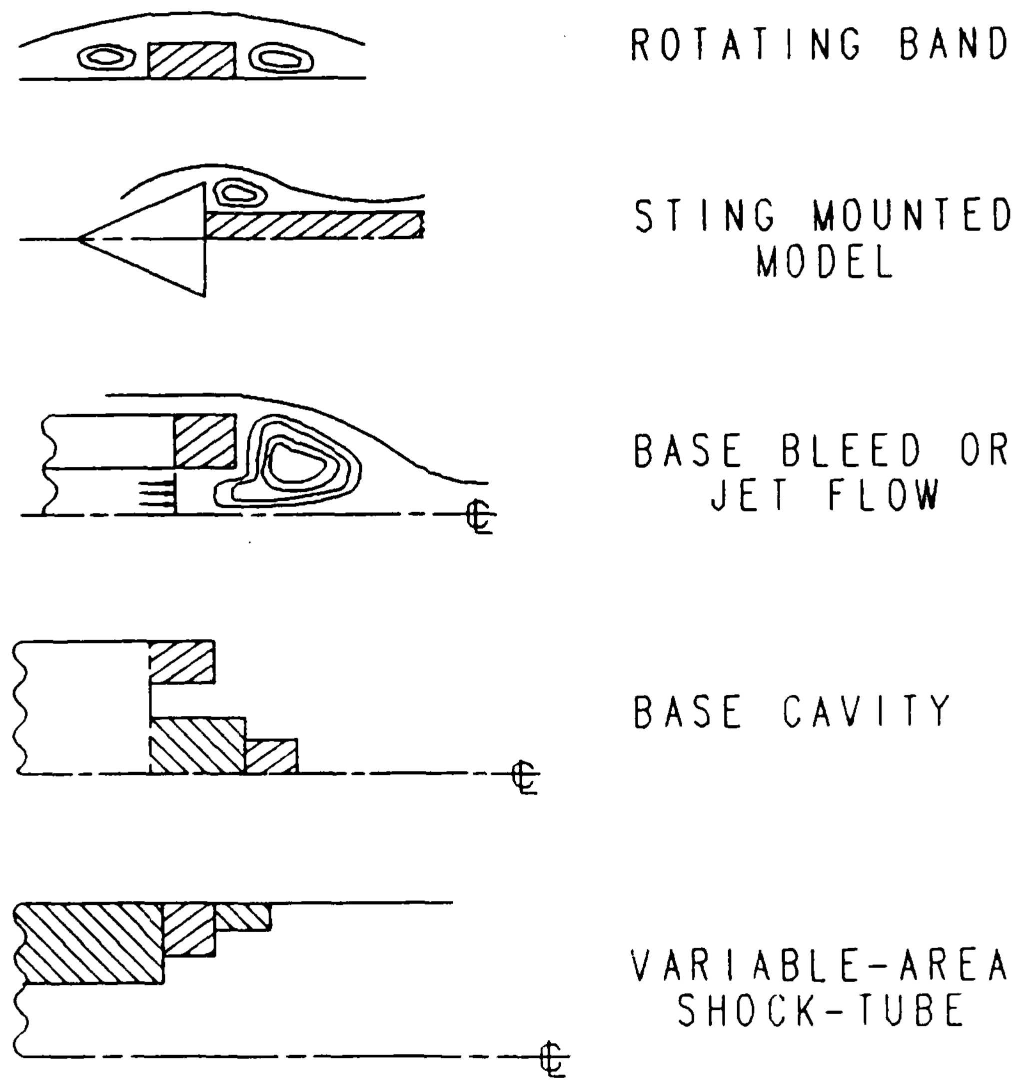

Figure 1. Examples of flowfield blanking.

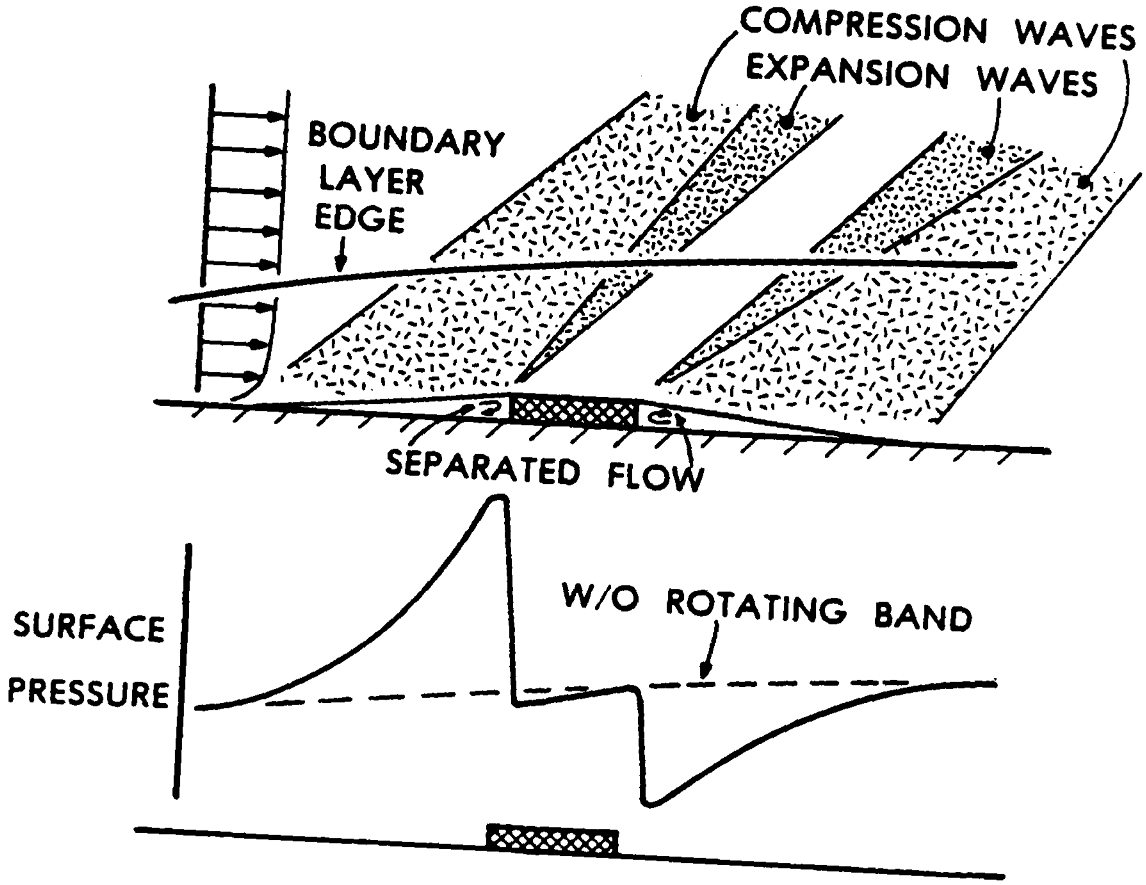

Figure 2. Schematics of rotating band flowfield.

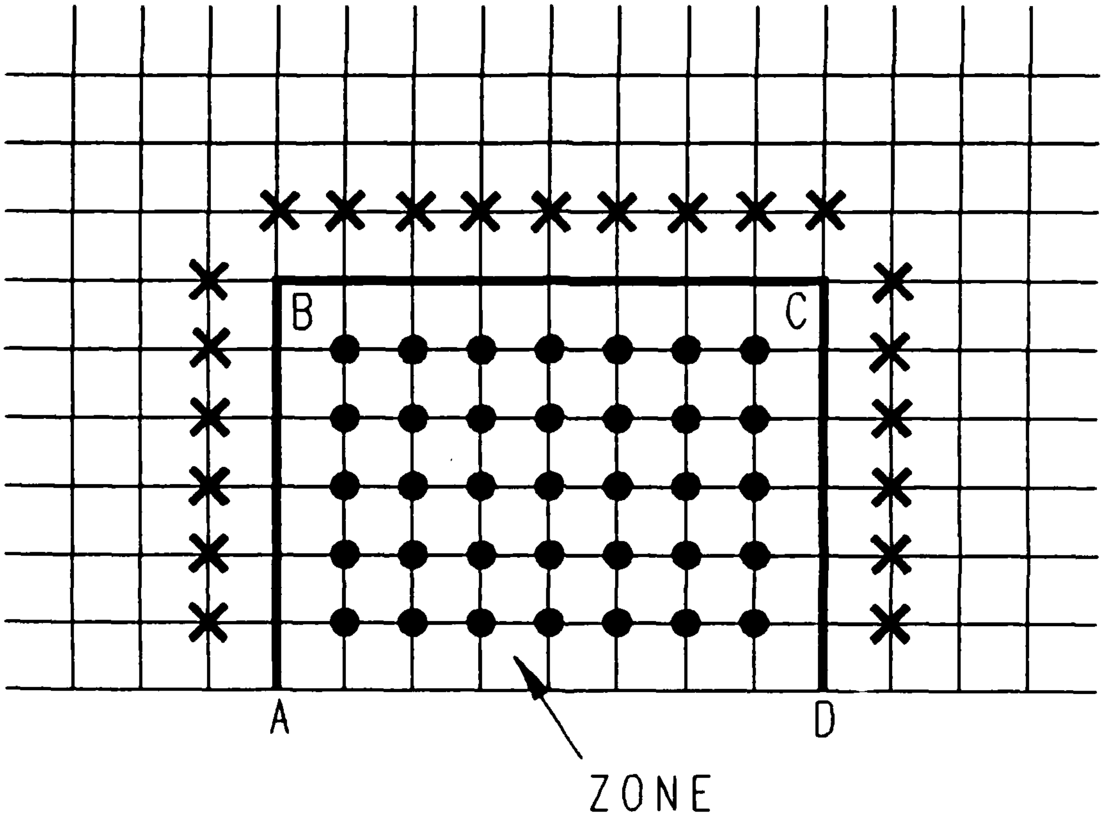

Figure 3. Schematic illustration of flowfield blanking.

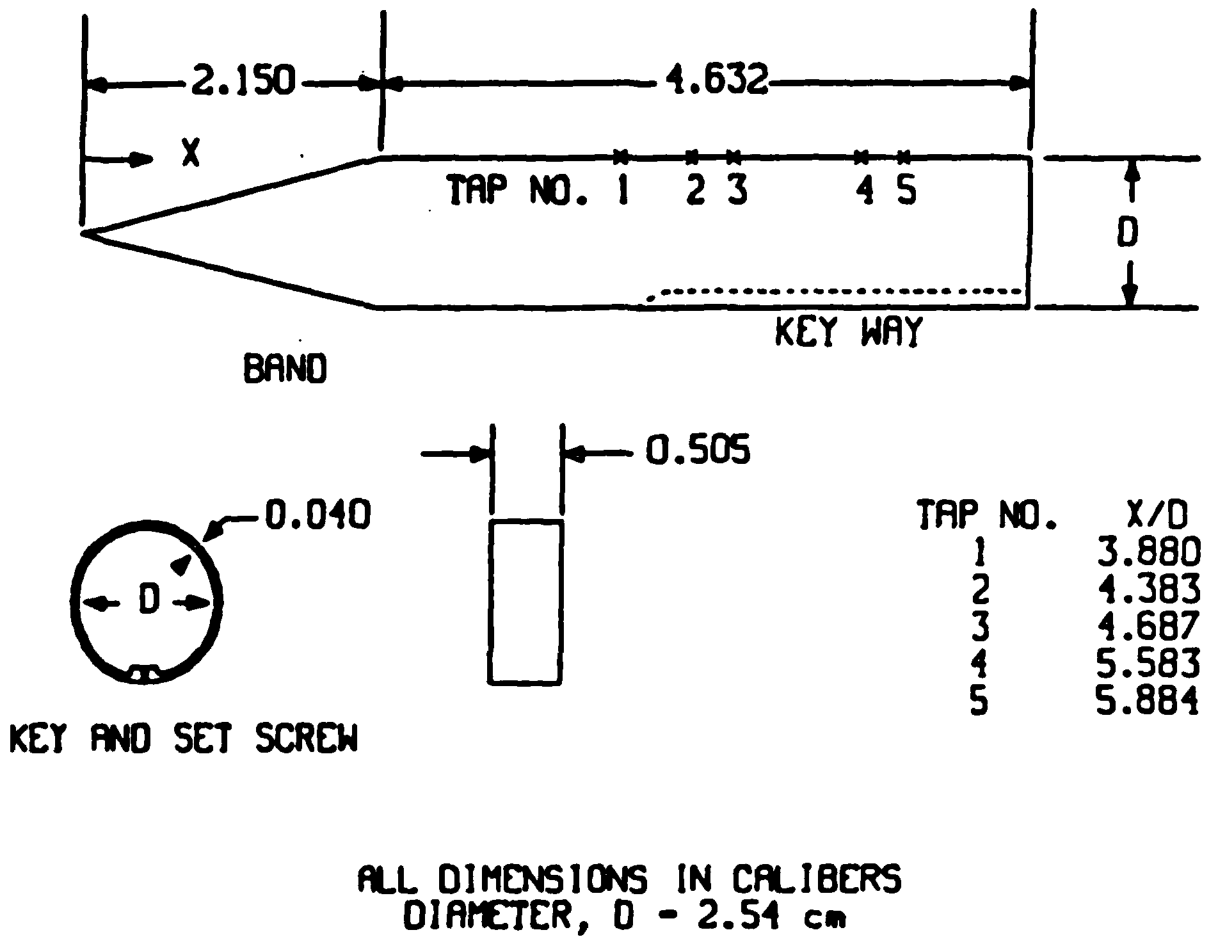

Figure 4. Model geometry.

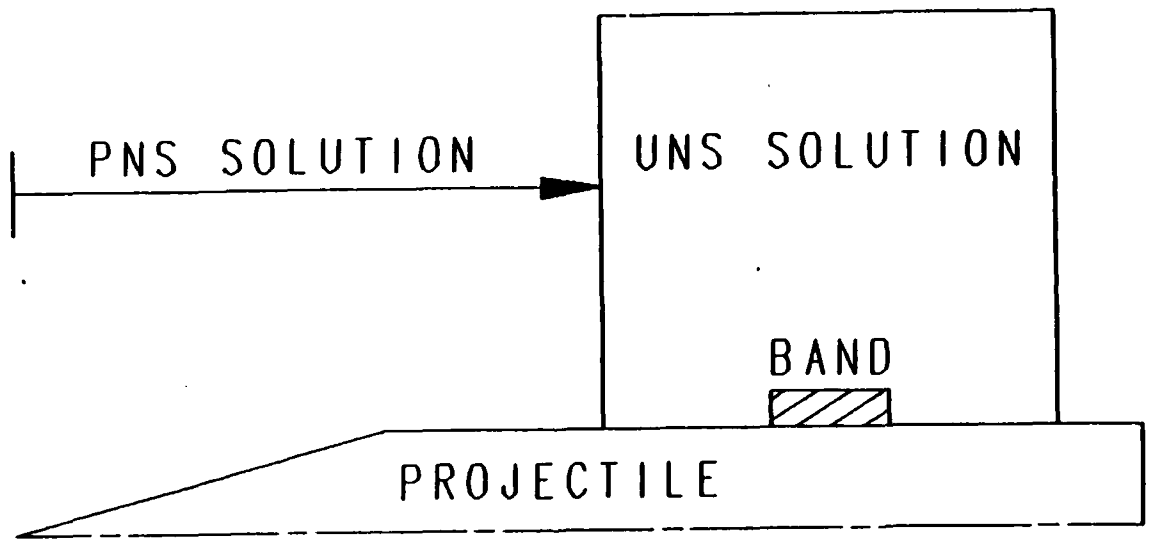

Figure 5. Composite solution technique.

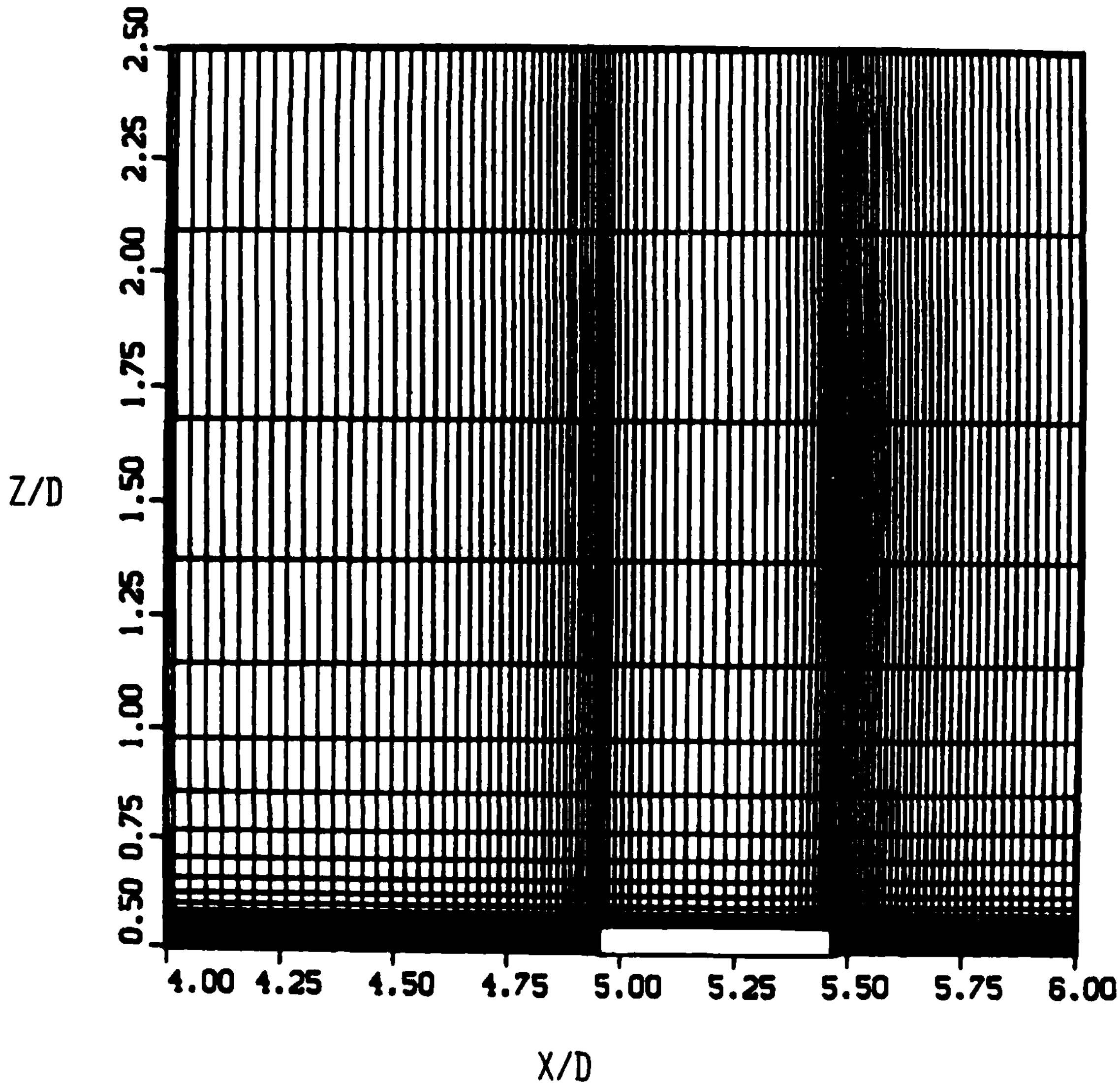

Figure 6. Computational grid expanded near the model.

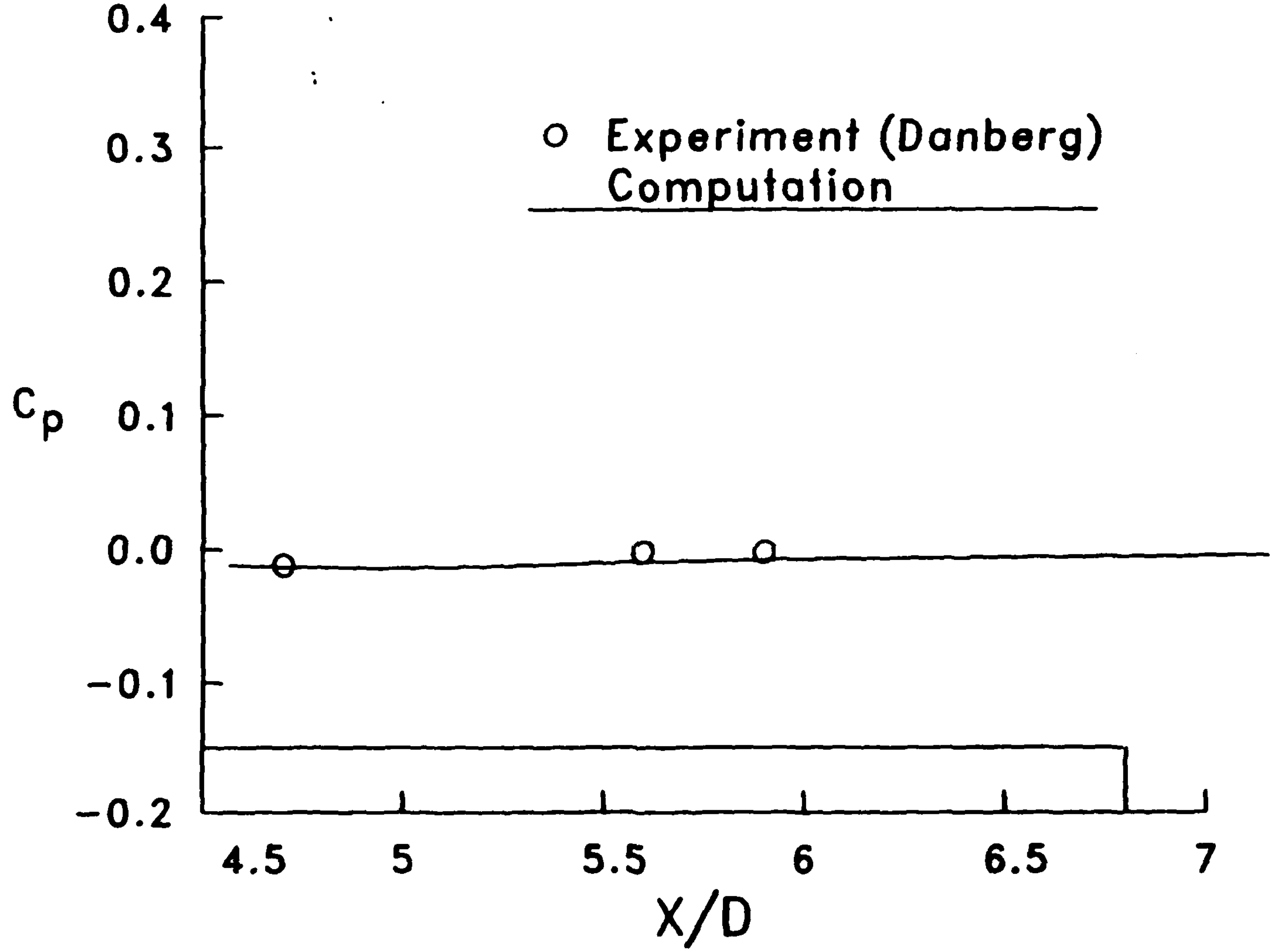

Figure 7. Longitudinal surface pressure distribution, $M_\infty = 3.0$, $\alpha = 0$ (without the band).

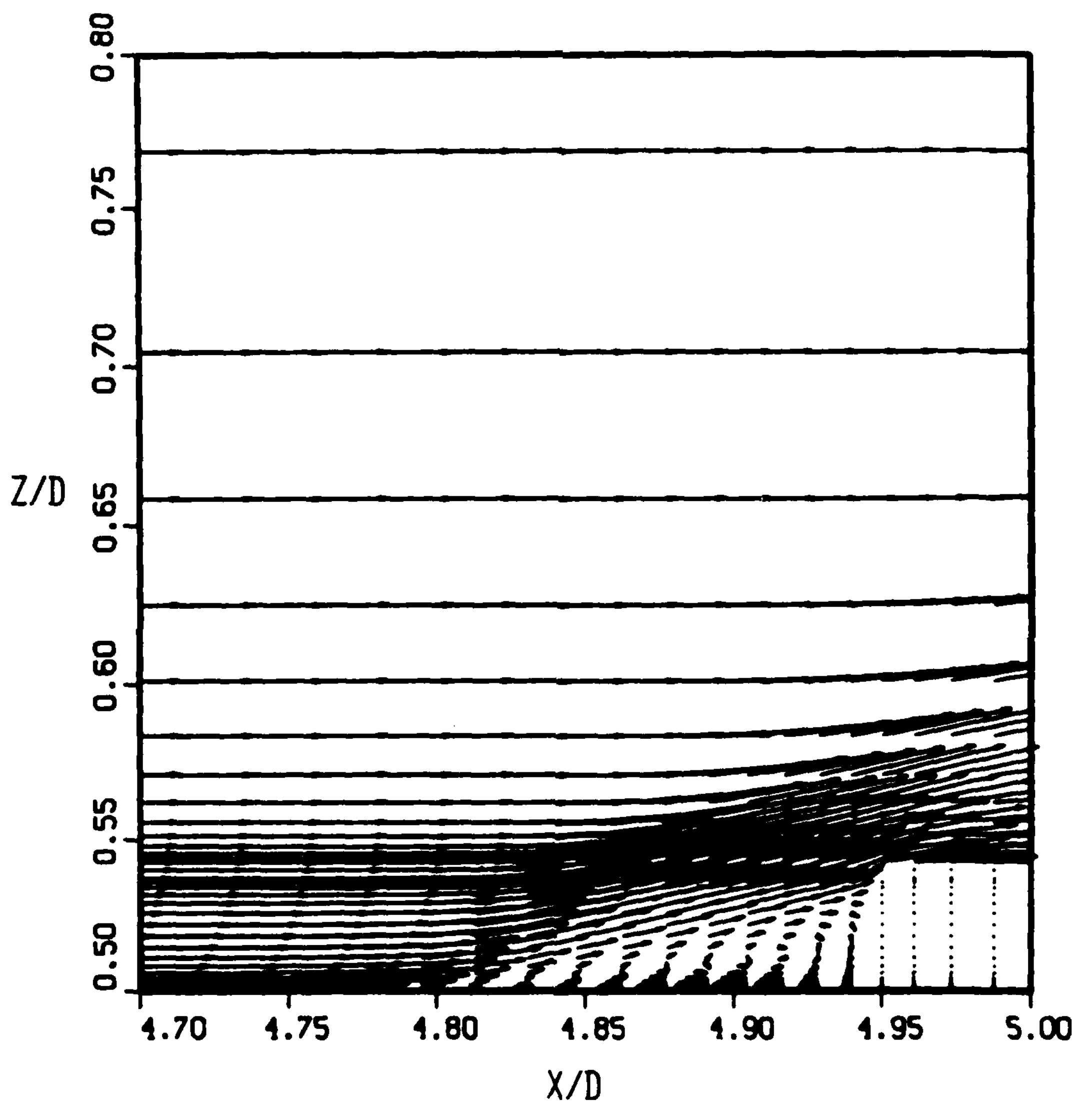

Figure 8a. Velocity vectors Ahead of the band, $M_\infty = 3.0$, $\alpha = 0$.

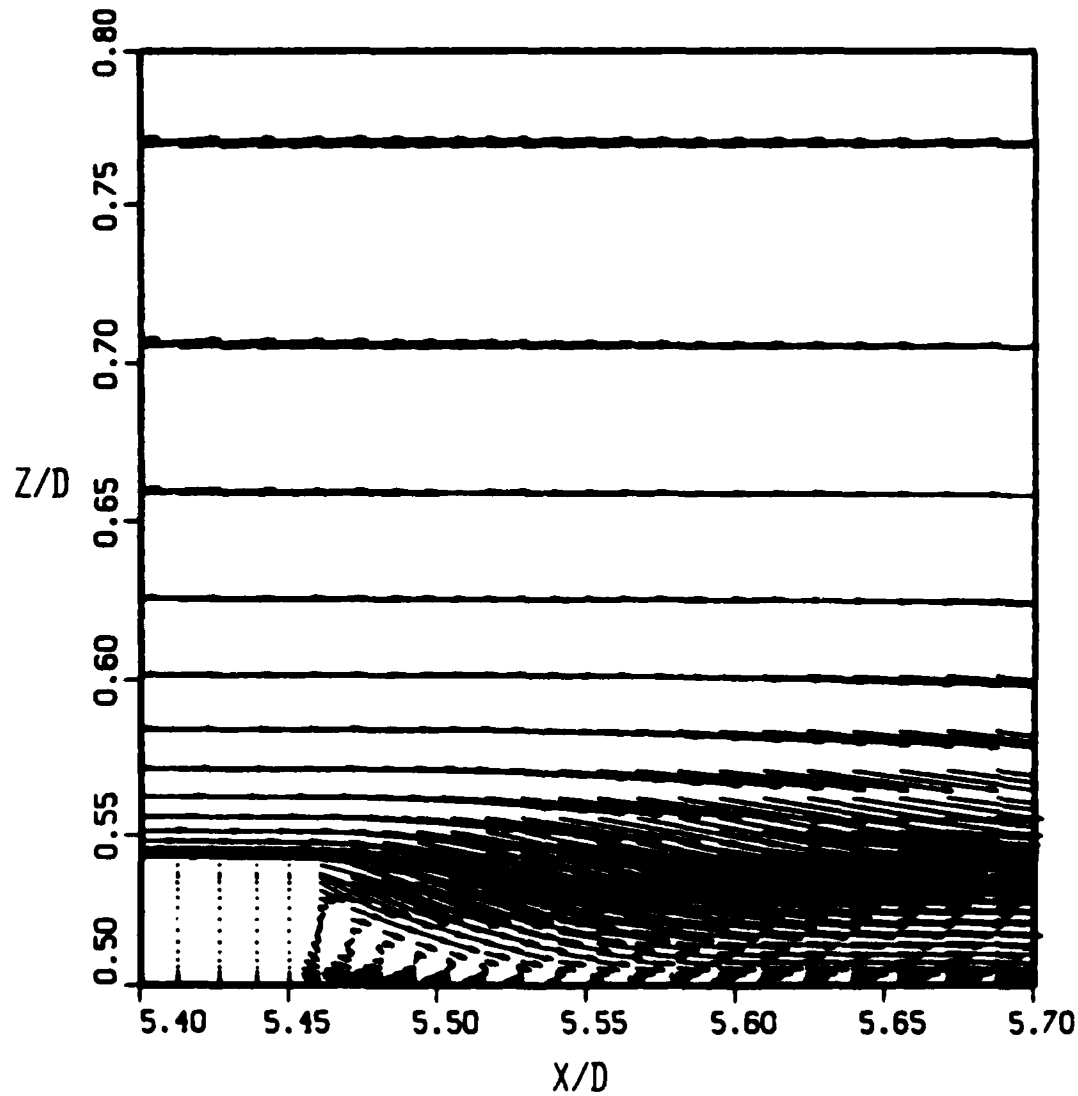

Figure 8b. Velocity vectors behind the band, $M_\infty = 3.0$, $\alpha = 0$.

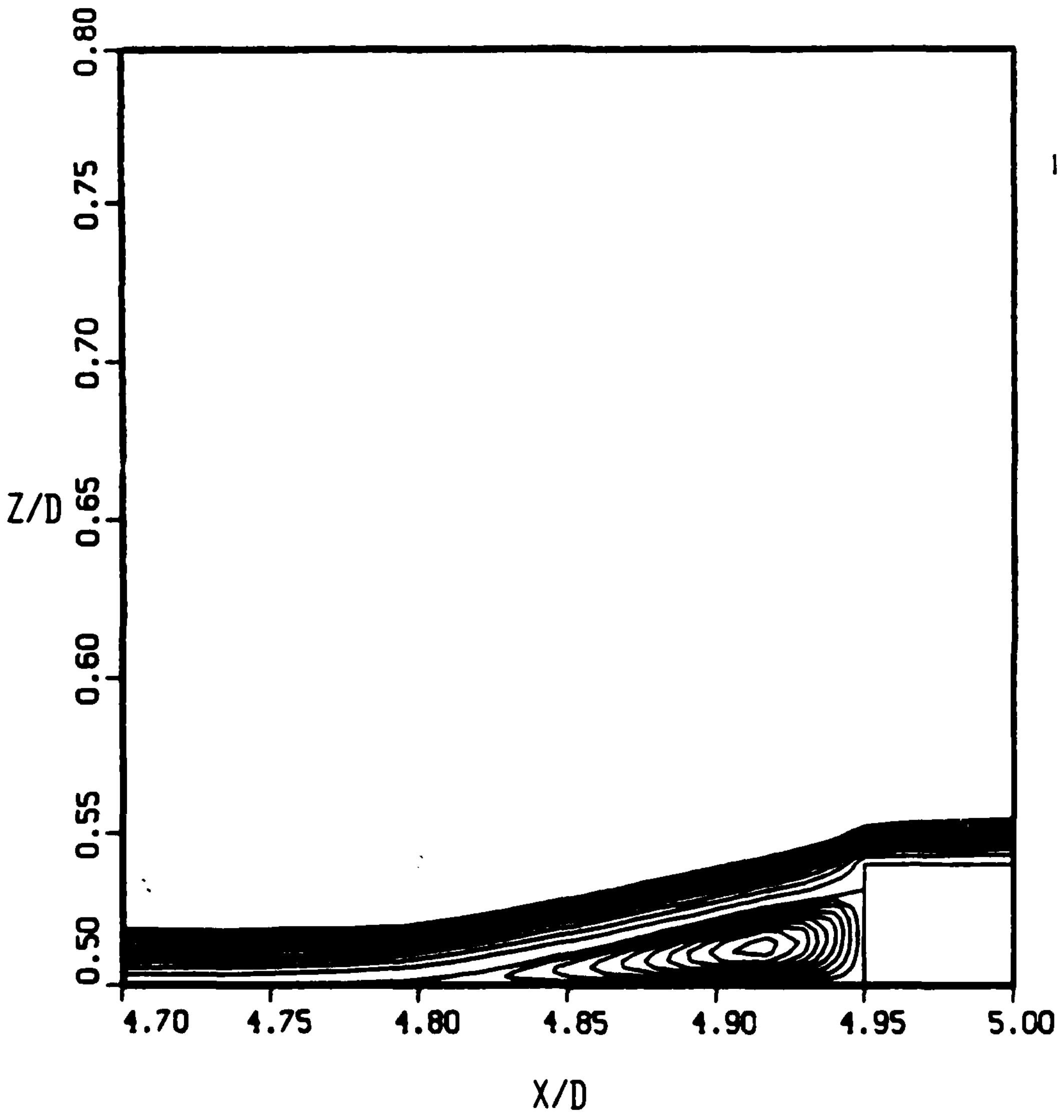

Figure 9a. Stream function contours ahead of the band, $M_\infty = 3.0$, $\alpha = 0$.

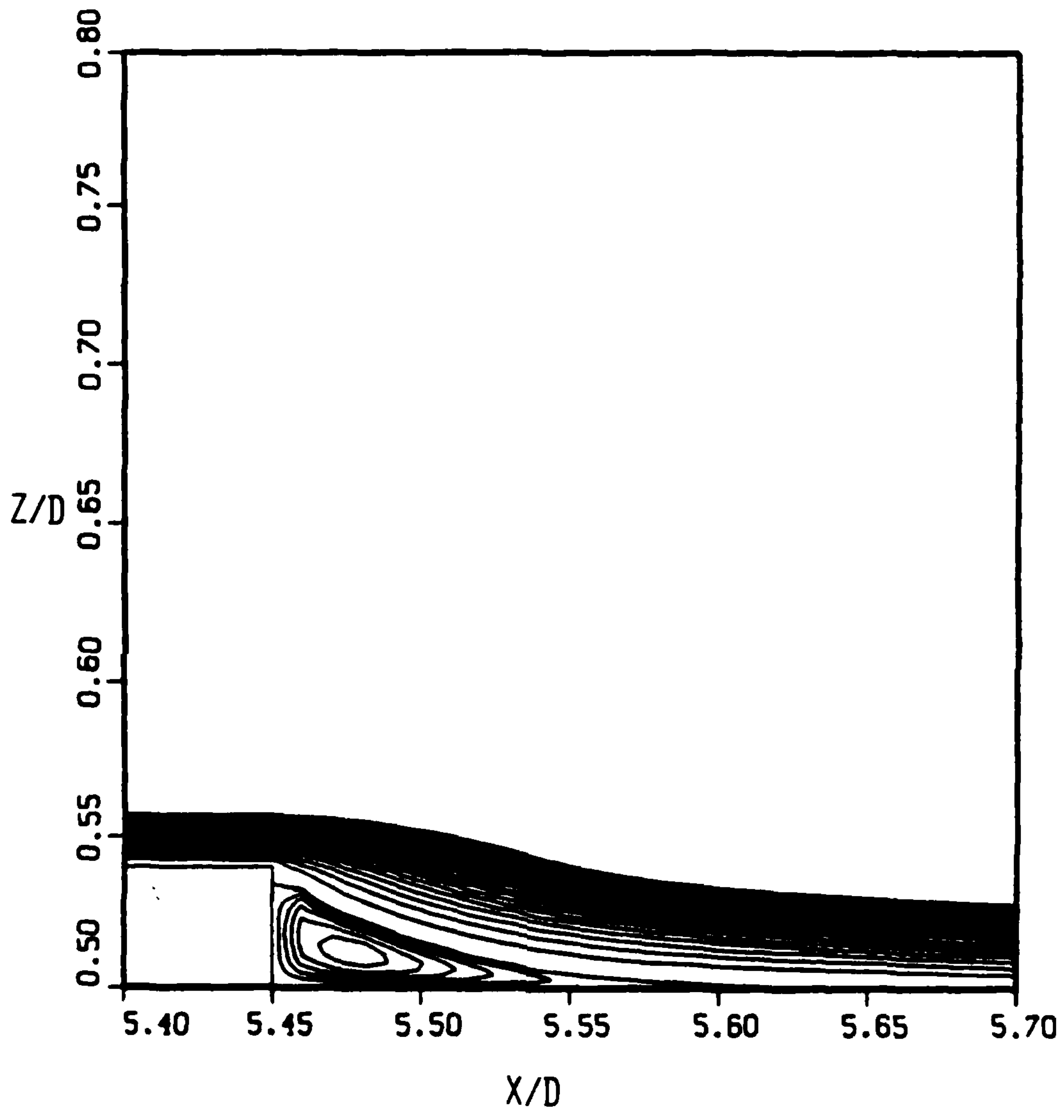

Figure 9b. Stream function contours behind the band, $M_\infty = 3.0$, $\alpha = 0$.

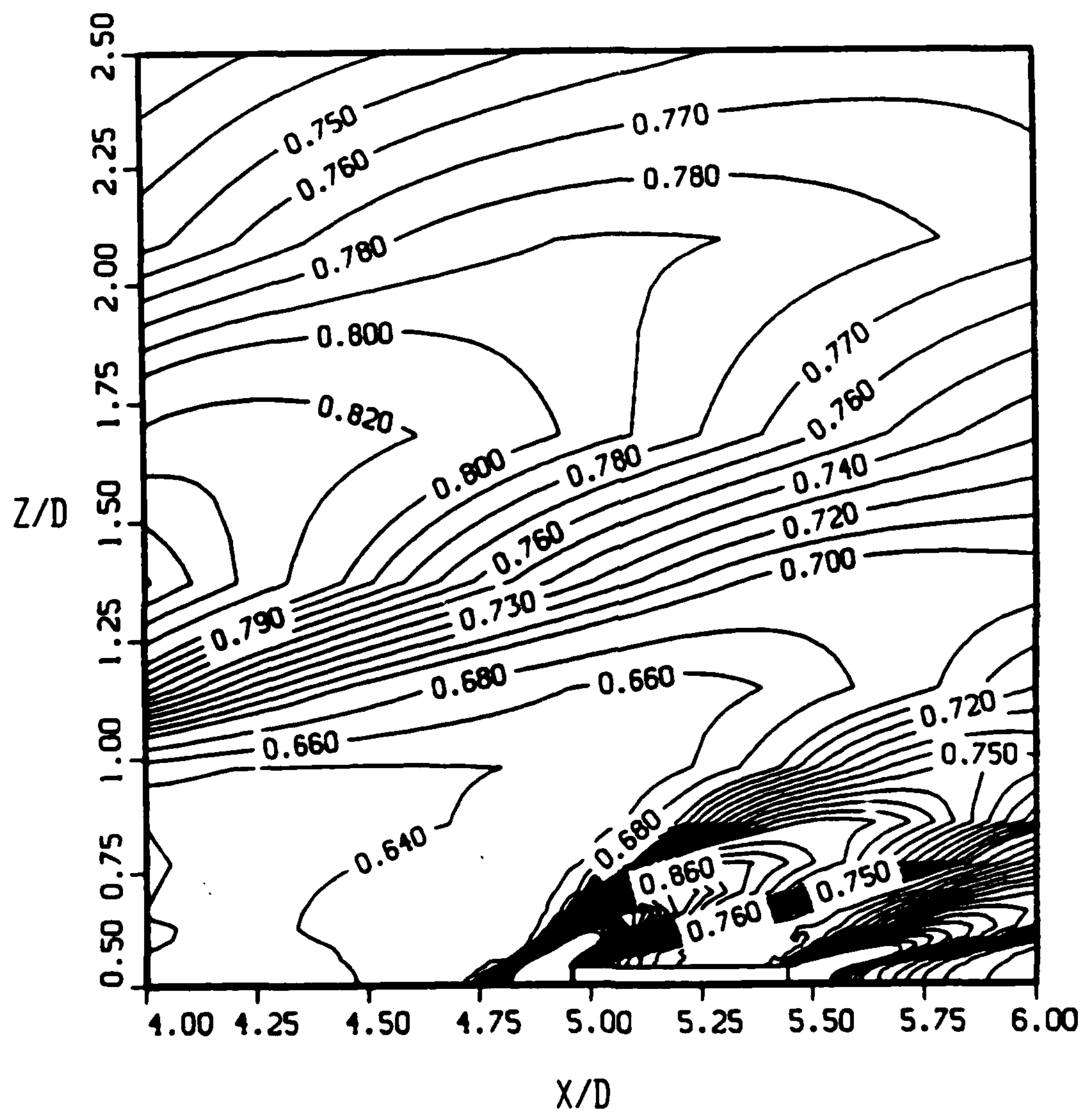

Figure 10. Pressure contours, $M_\infty = 3.0$, $\alpha = 0$.

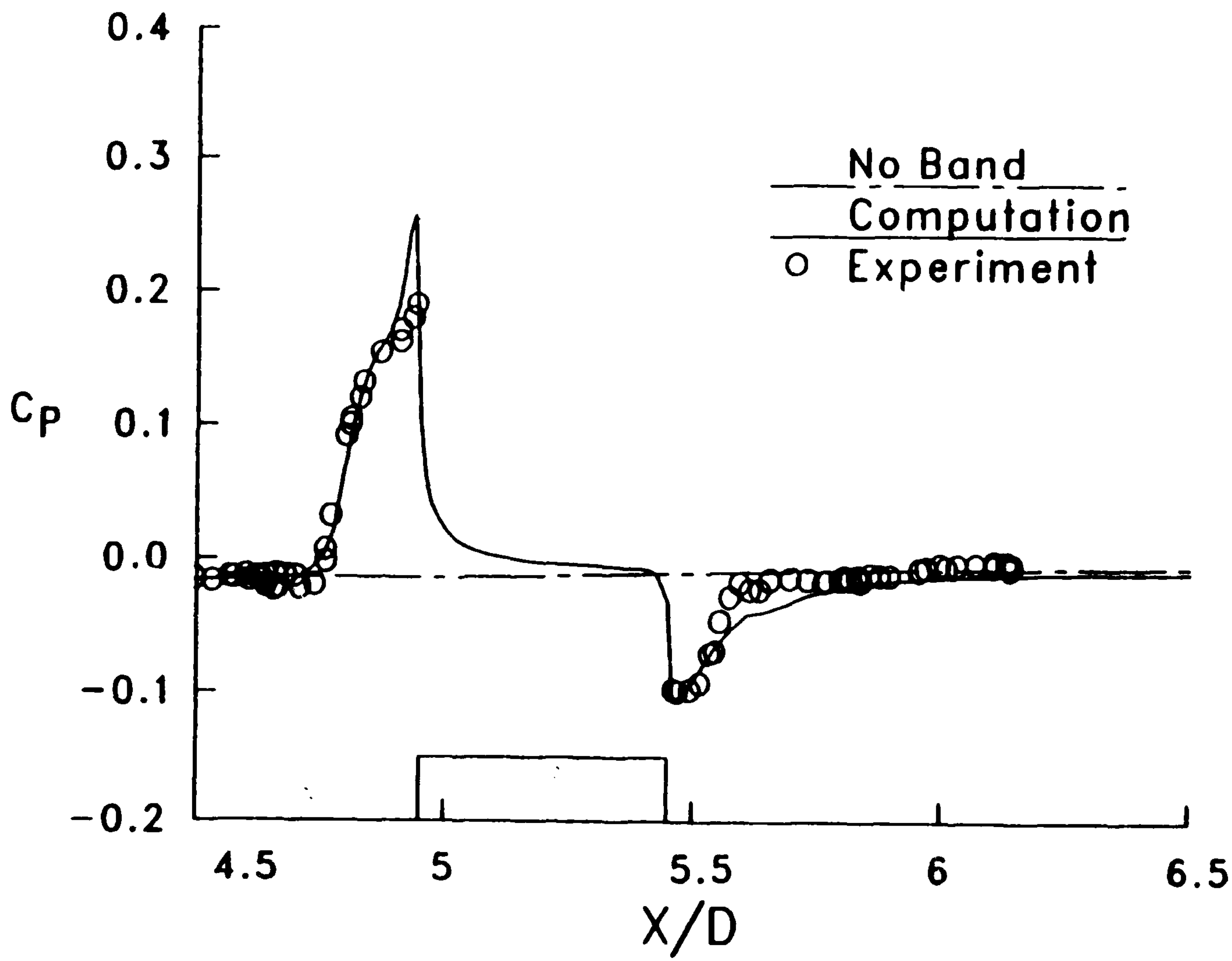

Figure 11. Longitudinal surface pressure distribution, $M_\infty = 3.0$, $\alpha = 0$ (with the band).

REFERENCES

1. Nietubicz, C.J., Pulliam, T.H. and Steger, J.L., "Numerical Solution of the Azimuthal-Invariant Navier-Stokes Equations," ARBRL-TR-02227, US Army Ballistic Research Laboratory, Aberdeen Proving Ground, Maryland, March 1980. (AD A085716) (Also see AIAA Journal, Vol. 18, No. 12, December 1980, pp. 1411-1412)

2. Nietubicz, C.J., "Navier-Stokes Computations for Conventional and Hollow Projectile Shapes at Transonic Velocities," ARBRL-MR-03184, US Army Ballistic Research Laboratory, Aberdeen Proving Ground, Maryland, July 1982. (AD A116866)

3. Sturek, W.B. and Schiff, L.B., "Numerical Simulation of Steady Supersonic Flow Over Spinning Bodies of Revolution," AIAA Journal, Vol. 20, No. 12, December 1982, pp. 1724-1731.

4. Sahu, J., Nietubicz, C.J. and Steger, J.L., "Navier-Stokes Computations of Projectile Base Flow with and without Base Injection," ARBRL-TR-02532, US Army Ballistic Research Laboratory, Aberdeen Proving Ground, Maryland, November 1983. (AD A135738) (Also see AIAA Journal, Vol. 23, No. 9, September 1985, pp. 1348-1355.

5. Sahu, J., "Supersonic Flow over Cylindrical Afterbodies with Base Bleed," ARBRL-TR-2742, US Army Ballistic Research Laboratory, Aberdeen Proving Ground, Maryland, June 1986.

6. Beam, R. and Warming, R.F., "An Implicit Factored Scheme for the Compressible Navier-Stokes Equations," AIAA Paper No. 77-645, June 1977.

7. Steger, J.L., "Implicit Finite Difference Simulation of Flow About Arbitrary Geometries with Application to Airfoils," AIAA Journal, Vol. 16, No. 4, July 1978, pp. 679-686.

8. Pulliam, T.H. and Steger, J.L., "On Implicit Finite-Difference Simulations of Three-Dimensional Flow," AIAA Journal, Vol. 18, No. 2, February 1980, pp. 159-167.

9. Pulliam, T.H., "Artificial Dissipation Models for the Euler Equations," AIAA Paper No. 85-0438, January 1985.

10. Baldwin, B.S. and Lomax, H., "Thin-Layer Approximation and Algebraic Model for Separated Turbulent Flows," AIAA Paper No. 78-257, 1978.

11. Danberg, J.E. and Palko, K.L., "Measurement of Surface Pressures Caused by a Projectile Rotating Band at Supersonic Speeds," ARBRL-MR-3532, US Army Ballistic Research Laboratory, Aberdeen Proving Ground, Maryland, July 1986.

LIST OF SYMBOLS

a = speed of sound

c_p = specific heat at constant pressure

C_p = pressure coefficient, $2(\rho_\infty a_\infty^2 p - p_\infty)/\rho_\infty u_\infty^2$

D = body diameter

e = total energy per unit volume/$\rho_\infty a_\infty^2$

$\hat{E}$, $\hat{F}$, $\hat{q}$ = flux vector of tranformed Navier-Stokes equations

$\hat{H}$ = η-invariant source vector

J = Jacobian of transformation

M = Mach number

p = pressure/$\rho_\infty a_\infty^2$

Pr = Prandtl number, $\mu_\infty c_p/\kappa_\infty$

R = body radius

Re = Reynolds number, $\rho_\infty a_\infty D/\mu_\infty$

$\hat{S}$ = viscous flux vector

t = physical time

u,v,w = Cartesian velocity components/a_∞

U,V,W = contravariant velocity components/a_∞

x,y,z = physical Cartesian coordinates

α = angle of attack

γ = ratio of specific heats

κ = coefficient of thermal conductivity/κ_∞

μ = coefficient of viscosity/μ_∞

ξ,η,ζ = transformed coordinates in axial, circumferential and radial directions

ρ = density/ρ_∞

Δ = forward difference

LIST OF SYMBOLS (Continued)

∇	=	backward difference
δ	=	central difference
τ	=	transformed time
ε_i	=	implicit smoothing coefficient
ε_d	=	second order dissipation coefficient
ε_e	=	fourth order dissipation coefficient

Superscript

*	=	critical value

Subscript

j	=	longitudinal direction
I	=	identity matrix
∞	=	free stream conditions for corresponding dimensional quantity
ξ	=	streamwise direction
ζ	=	normal direction

DISTRIBUTION LIST

No. of Copies	Organization
12	Administrator Defense Technical Info Center ATTN: DTIC-FDAC Cameron Station, Bldg 5 Alexandria, VA 22304-6145
1	HQDA DAMA-ART-M Washington, DC 20310
1	Commander US Army Materiel Command ATTN: AMCDRA-ST 5001 Eisenhower Avenue Alexandria, VA 22333-0001
5	Commander Armament RD&E Center US Army AMCCOM ATTN: SMCAR-MSI SMCAR-LCA-F/Mertz Loeb Hudgins Friedman Dover, NJ 07801-5001
1	Commander US Army Armament, Munitions & Chemical Command ATTN: SMCAR-IMP-L Rock Island, IL 61299-7300
1	Commander US Army Armament, Research, Development & Engineering Ctr ATTN: SMCAR-TDC Dover, NJ 07801
1	Commander US Army Jefferson Proving Ground Materiel Testing Directorate ATTN: Arthur B. Alphin, MAJ, ARM Madison, IN 47250-5100
1	Commander CECOM R&D Technical Library ATTN: AMSEL-IM-L Fort Monmouth, NJ 07703-5000
1	Director US AMCCOM ARDEC CCAC Benet Weapons Laboratory ATTN: SMCAR-CCB-TL Watervliet, NY 12189-4050
1	Commander US Army Aviation Systems Cmd ATTN: AMSAV-E 4300 Goodfellow Blvd. St. Louis, MO 63120-1798
1	Director US Army Aviation Research & Technology Activity Ames Research Center Moffett Field, CA 94035-1099
3	Commander US Army Missile Command ATTN: AMSMI-RX Redstone Arsenal, AL 35898-5249
1	Director US Army Missile & Space Intelligence Center ATTN: AIAMS-YDL Redstone Arsenal, AL 35898-5500
1	Commander US Army Tank Automotive Command ATTN: AMSTA-TSL Warren, MI 48397-5500
1	Director US Army TRADOC Analysis Center ATTN: ATOR-TSL White Sands Missile Range, NM 88002-5502
1	Commander US Army Research Office P. O. Box 12211 Research Triangle Park, NC 27709

DISTRIBUTION LIST

No. of Copies	Organization
1	Commander US Naval Air Systems Command ATTN: AIR-604 Washington, DC 20360
2	Commander US Naval Surface Weapons Center ATTN: Dr. T. Clare, Code DK20 Dr. F. Moore Dahlgren, VA 22448-5000
1	Commander US Naval Surface Weapons Center ATTN: Dr. U. Jettmar Silver Spring, MD 20902-5000
1	Commander US Naval Weapons Center ATTN: Code 3431, Tech Lib China Lake, CA 93555
1	Commander US Army Development & Employment Agency ATTN: MODE-ORO Ft. Lewis, WA 98433-5000
1	Director NASA Langley Research Center ATTN: NS-185, Tech Lib Langley Station Hampton, VA 23365
4	Director NASA Ames Research Center ATTN: MS-202-1/Pulliam Steger MS-227-8/Schiff Moffett Field, CA 94035
2	Commandant US Army Infantry School ATTN: ATSH-CD-CS-OR Ft. Benning, GA 31905
1	Commandant USAFAS ATTN: ATSF-TSM-CN Ft. Sill, OK 73503-5600
1	AFWL/SUL Kirtland AFB, NM 87117
1	AFATL/DOIL (Tech Info Ctr) Eglin AFB, FL 32542-5438
2	Sandia Laboratories ATTN: Dr. W.L. Oberkampf Dr. F. Blottner Division 1636 Sandia National Laboratories Albuquerque, NM 87185
1	AEDC Calspan Field Services ATTN: MS 600 (Dr. John Benek) AAFS, TN 37389
1	Virginia Polytechnic Institute & State University ATTN: Dr. Clark H. Lewis Department of Aerospace & Ocean Engineering Blacksburg, VA 24061
1	University of California, Davis Department of Mechanical Engineering ATTN: Prof. H.A. Dwyer Davis, CA 95616
1	Pennsylvania State University Department of Aerospace Engineering ATTN: Dr. G. S. Dulikravich University Park, PA 16802
1	University of Florida Dept. of Engineering Sciences College of Engineering ATTN: Prof. C. C. Hsu Gainesville, FL 32611
10	CIA OIR/DB/Standard GE47 HQS Washington, DC 20505

DISTRIBUTION LIST

No. of Copies	Organization
1	University of Illinois at Urbana Champaign Department of Mechanical & Industrial Engineering ATTN: Prof. W. L. Chow Urbana, IL 61801
1	University of Maryland Department of Aerospace Engineering ATTN: Dr. J.D. Anderson, Jr. College Park, MD 20742
1	University of Notre Dame Department of Aeronautical & Mechanical Engineering ATTN: Prof. T.J. Mueller Notre Dame, IN 46556
1	University of Texas Department of Aerospace Engineering & Engineering Mechanics ATTN: Dr. D.S. Dolling Austin, Texas 78712-1055
	<u>Aberdeen Proving Ground</u>
	Dir, USAMSAA ATTN: AMXSY-D AMXSY-MP, H. Cohen
	Cdr, USATECOM ATTN: AMSTE-SI-F
	Cdr, CRDEC, AMCCOM ATTN: SMCCR-RSP-A SMCCR-MU SMCCR-SPS-IL

USER EVALUATION SHEET/CHANGE OF ADDRESS

This Laboratory undertakes a continuing effort to improve the quality of the reports it publishes. Your comments/answers to the items/questions below will aid us in our efforts.

1. BRL Report Number ______________________ Date of Report ____________

2. Date Report Received ____

3. Does this report satisfy a need? (Comment on purpose, related project, or other area of interest for which the report will be used.) ______________________

4. How specifically, is the report being used? (Information source, design data, procedure, source of ideas, etc.) ______________________

5. Has the information in this report led to any quantitative savings as far as man-hours or dollars saved, operating costs avoided or efficiencies achieved, etc? If so, please elaborate. ______________________

6. General Comments. What do you think should be changed to improve future reports? (Indicate changes to organization, technical content, format, etc.)

CURRENT ADDRESS

Name

Organization

Address

City, State, Zip

7. If indicating a Change of Address or Address Correction, please provide the New or Correct Address in Block 6 above and the Old or Incorrect address below.

OLD ADDRESS

Name

Organization

Address

City, State, Zip

(Remove this sheet along the perforation, fold as indicated, staple or tape closed, and mail.)

— — — — — — — — — FOLD HERE — — — — — — — — — — —

Director
U.S. Army Ballistic Research Laboratory
ATTN: SLCBR-DD-T
Aberdeen Proving Ground, MD 21005-5066

NO POSTAGE
NECESSARY
IF MAILED
IN THE
UNITED STATES

OFFICIAL BUSINESS
PENALTY FOR PRIVATE USE, $300

BUSINESS REPLY MAIL
FIRST CLASS PERMIT NO 12062 WASHINGTON, DC

POSTAGE WILL BE PAID BY DEPARTMENT OF THE ARMY

Director
U.S. Army Ballistic Research Laboratory
ATTN: SLCBR-DD-T
Aberdeen Proving Ground, MD 21005-9989

— — — — — — — — — FOLD HERE — — — — — — — — — — —

END

4-87

DTIC